Computational Treatment of Three-Dimensional Transonic Canard-Wing Interactions

Vijaya Shankar* and Norman Malmuth†
Rockwell International Science Center, Thousand Oaks, California

The transonic canard-wing interaction problem is simulated using the modified small disturbance transonic theory. The wing and the canard are treated in a sheared fine grid system that is embedded in a global Cartesian crude grid. An appropriate far field and asymptotic expression for the velocity potential derived using Green's theorem is implemented. Results are presented for a few canard-wing configurations and compared with available experimental data. The weakening of the wing shock due to the presence of the canard downwash is illustrated in terms of contour plots. An empirical incidence correction for the wing leading-edge vortex gives good agreement with experiment at low incidences. For higher angles of attack, the results indicate that a more sophisticated vortex roll-up and induction model is required.

Introduction

A NUMBER of highly maneuverable fighter configurations have been proposed with closely coupled canard systems which can lead to several advantages such as higher trimmed-lift capability, improved pitching moment characteristics, and reduced trim drag. The associated interaction due to such surfaces with the wing as well as those from conventional tail planes involves important nonlinear phenomena in the supercritical speed regime. These effects can significantly change spanwise load distributions as well as the effective incidence field. Corresponding modifications of aerodynamic performance and stability characteristics are therefore to be anticipated not only for fighter configurations, but with tails interacting with large-aspect-ratio wings typical of transport arrangements as well.

To understand clearly the closely coupled canard-wing interference transonic flowfields with emphasis on benefits associated with longitudinal and lateral positioning that have been discussed by Gloss and Washburn,[1] it is essential to develop a computational model that properly simulates the full nonlinear coupling of both surfaces. In this respect, the mutual induction arises naturally in the computational model in contrast to other "immersion" techniques which have been advocated. The latter employs an iterative procedure in which each surface's isolated aerodynamics is alternately corrected for induction from the other. This concept may have some validity for large stagger and gap cases, but may not converge for closely coupled arrangements. In fact, even if convergence is obtained, the result may not be the physically correct solution.

A mutually interacting two-dimensional canard-wing model based on the Karman-Guderley transonic small disturbance theory is reported in Ref. 2 showing several parametric studies involving canard-wing angles of attack, stagger, and gap between the two lifting elements. The objective of the present study is to extend the two-dimensional analysis to three dimensions by modifying an existing small disturbance theory transonic code for wing-body combinations[3] to include the presence of a canard or tail. The approach is to introduce a separate sheared fine grid box for the canard similar to the one used for the wing. However, the experience from the two-dimensional analysis[2] indicates that erroneous solutions can result from the use of two fine grid box arrangements for very closely coupled canard-wing systems due to placement of the outer boundaries of the fine grid box in strong nonlinear regions of the other surface. To avoid this situation, when the canard is in the close proximity of the wing, a single fine grid box is used that encloses both the lifting surfaces. By contrast, the two fine grid box arrangement is used for mildly coupled canard-wing configurations. Besides the numerical implementation, the paper also includes a detailed analysis of the appropriate far-field procedure based on an asymptotic theory. The present paper neglects the downward deflection of the wake, vortex roll-up, and leading-edge separation phenomena. These can be important effects and are being considered in separate analyses.

Results are shown for a few sample canard-wing configurations and compared with available experimental data.

Presented as Paper 82-0161 at the AIAA 20th Aerospace Sciences Meeting, Orlando, Fla., Jan. 11-14, 1982; submitted Feb. 5, 1982; revision received Aug. 9, 1982.

*Program Manager, Computational Fluid Dynamics. Associate Fellow AIAA.

†Member Technical Staff. Associate Fellow AIAA.

Equations and Boundary Conditions

The modified form of the transonic classical small disturbance theory, in conservation form as used in Ref. 3, will be employed in the current formulation of the canard/tail problem:

$$\left[(1-M_\infty^2)\phi_x - \frac{\gamma+1}{2}M_\infty^{1.75}\phi_x^2 + \left(\frac{\gamma-3}{2}\right)M_\infty^2\phi_y^2\right]_x + [\phi_y - (\gamma-1)M_\infty^2\phi_x\phi_y]_y + [\phi_z]_z = 0 \tag{1}$$

The above equation is in the conservation form usually preferred for better shock resolution. Use of Eq. (1) allows one to apply the wing and canard surface boundary conditions at their respective mean chord planes and to transfer boundary conditions on the fuselage to a convenient computational prismatic surface. Referring to Fig. 1, the boundary conditions on the wing and canard mean plane are given by

$$\phi_z(x,y;z_{w,c}\pm) = \frac{1}{M_\infty^{0.25}}\left\{\frac{dZ_{w,c}(x,y;z_{w,c}\pm)}{dx} - \alpha\right\} \tag{2}$$

where $z=z_{w,c}\pm$ defines the wing and canard mean planes, with the plus sign denoting the upper surface and the minus sign the lower surface. The wing and canard shapes are prescribed by $Z_{w,c}(x,y)$. Application of boundary conditions on the mean planes avoids the need for body-fitted mapping procedures. The subscripts w and c denote the wing and canard, respectively.

Across the vortex wake, there will be a jump in the velocity potential ϕ which will be incorporated into the calculation as a boundary condition while solving Eq. (1) at grid points neighboring the wake. The wake jump condition is

$$[\phi]_{\text{wing}} = \phi(x,y,z_w+) - \phi(x,y,z_w-) = \Gamma_w(y) \qquad x \geq x_{\text{TE},w}$$

$$[\phi]_{\text{canard}} = \phi(x,y,z_c+) - \phi(x,y,z_c-) = \Gamma_c(y) \qquad x \geq x_{\text{TE},c} \tag{3}$$

where x_{TE} prescribes the trailing-edge shape, and $\Gamma_x(y)$ and $\Gamma_c(y)$ denote the sectional circulation given by

$$\Gamma_w(y) = \phi[x_{\text{TE},w}(y),y,z_w+] - \phi[x_{\text{TE},w}(y),y,z_w-]$$

$$\Gamma_c(y) = \phi[x_{\text{TE},c}(y),y,z_c+] - \phi[x_{\text{TE},c}(y),y,z_c-] \tag{4}$$

Transforming and Gridding

In general, canard-wing configurations will have different planform shapes for both lifting units, and, in particular, different leading- and trailing-edge sweeps. In order to treat arbitrary arrangements, it is essential to incorporate separate shearing transformations for both surfaces so as to unsweep them to rectangular planforms in a computational domain. This can be accomplished using the following shearing transformation:

$$\zeta_{w,c} = \frac{x - x_{\text{LE},w,c}(y)}{x_{\text{TE},w,c}(y) - x_{\text{LE},w,c}(y)}$$

$$\eta_{w,c} = y \qquad \xi_{w,c} = z \tag{5}$$

Since the transformation for the wing is different from the canard, the computational box containing the canard will be different from that containing the wing. This is illustrated in Fig. 2.

In order to establish a communication between the wing box and the canard box for data transfer from one to the other, a global crude grid will be set up which completely encloses both, as shown in Fig. 2. The global crude grid is in terms of the Cartesian system, while the canard and wing boxes are in terms of sheared coordinates represented by Eq. (5). To achieve a desired flow resolution for the two units, a very fine grid with clustering near the leading and trailing edges will be used in the canard and wing boxes. The Cartesian crude grid will extend several chord lengths from the configuration where far-field boundary conditions can be set. For very closely coupled canard-wing systems, the concept of two fine grid box arrangement can lead to erroneous solutions as well as numerical stability problems due to placement of the outer boundaries of the fine grid boxes in strong nonlinear regions of the other surface. This problem was experienced in the earlier two-dimensional analysis.[2] Thus, when a closely coupled canard-wing system is analyzed, a single fine grid box that encloses both the canard and the wing is used. (The single fine grid box has a shearing transformation based on the wing planform.) This is illustrated in Fig. 3. In this situation, the location of the canard leading and trailing edges within the wing sheared fine grid system is obtained by interpolation. The find grid may have to be specified manually to achieve desired grid clustering for the canard. The double fine grid box arrangement of Fig. 2 should work very well for mildly coupled canard-wing systems.

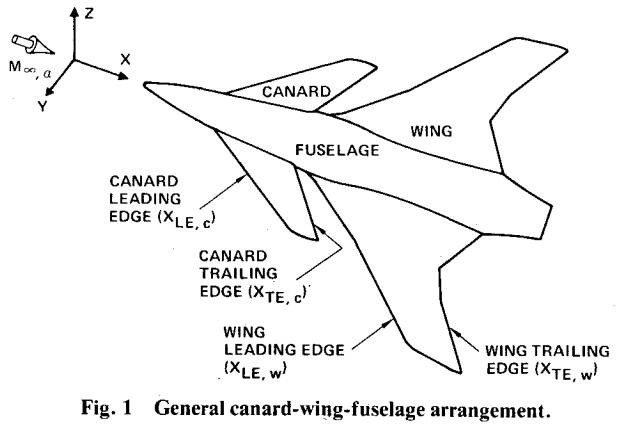

Fig. 1 General canard-wing-fuselage arrangement.

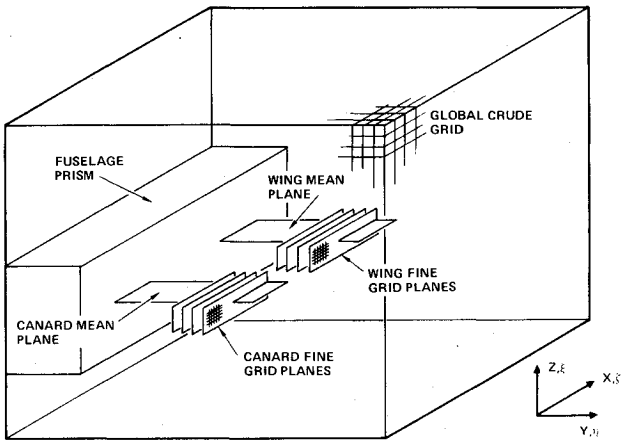

Fig. 2 Computational domain for the canard-wing-fuselage arrangement.

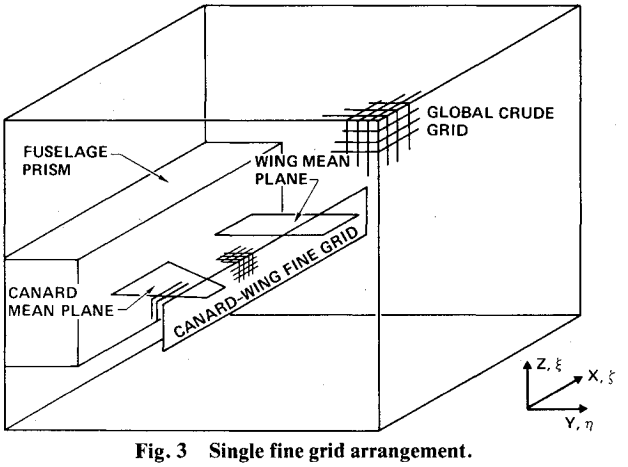

Fig. 3 Single fine grid arrangement.

Solution Procedure

Equation (1) in its Cartesian form is solved in the global crude grid while the transformed equation, in terms of the new variables, ζ, η, ξ, is solved in the fine grid box using a successive line overrelaxation algorithm. After each relaxation cycle along the crude grid/fine grid interface, the potential values from the crude grid are interpolated to the fine grid points and used as Dirichlet boundary condition for the fine grid box. Similarly, at the wing and canard mean planes, the potential values for the crude grid points are obtained from the grid values and provide a Dirichlet boundary condition for the crude grid domain. The use of crude grid/fine grid successive sweep procedure accelerates the convergence process.[4]

Far-Field Solution

Along the outer boundaries of the computational domain, it is important to use appropriate far-field boundary conditions. These will be obtained from a biwing generalization of the asymptotic analysis of Murman and Cole[5] for nonlifting airfoils and its three-dimensional wing extension by Klunker.[6]

A biwing system without a fuselage is shown in Fig. 4a. The far-field derivation procedure will be indicated for these elements, and an extension to inclusion of the fuselage will be briefly indicated. Shown in the figure is the canard surface, S_c, upstream of the main wing, S_w. Also depicted are the respective trailing vortex sheets, $S_v^{(c)}$ and S_v, of both elements. A $y=0$ projection of the compound lifting system is indicated in Fig. 4b.

For this derivation, we neglect the downward deflection of the wake for moderately large downstream locations of the computational approximation of the Trefftz plane boundary. Also neglected in this treatment are vortex roll-up and leading-edge separation phenomena.

Using the procedure from Refs. 5 and 6, the aforementioned integrodifferential equation for the velocity potential ϕ is obtained by applying Green's theorem to the small disturbance equation. The Karman-Guderley formulation is used to illustrate the basic method to be applied to a modified small disturbance (MSD) solver.[2] Using suitable strained coordinates (x,y,z) indicated in the figure and a corresponding set (ξ,η,ζ) for the dummy variables, the small disturbance equation for the perturbation potential ϕ in this system is

$$\nabla^2_{\xi,\eta,\zeta}\phi \equiv \frac{\partial^2\phi}{\partial\xi^2}+\frac{\partial^2\phi}{\partial\eta^2}+\frac{\partial^2\phi}{\partial\zeta^2}=A(\phi_\xi^2)_\xi$$
$$A\equiv(\gamma+1)/2 \tag{6}$$

For purposes of application of Green's theorem, a fundamental solution G is introduced which satisfies the following equation:

$$\nabla^2_{\xi,\eta,\zeta}G=\delta(\xi-x)\delta(\eta-y)\delta(\zeta-z) \tag{7}$$

Thus G is the usual unit source given by

$$G=-(1/4\pi R)$$
$$R^2=(x-\xi)^2+(y-\eta)^2+(z-\zeta)^2$$

Using Green's theorem on the domain cut along the approximate wake locations shown in Fig. 4b, i.e., the planes

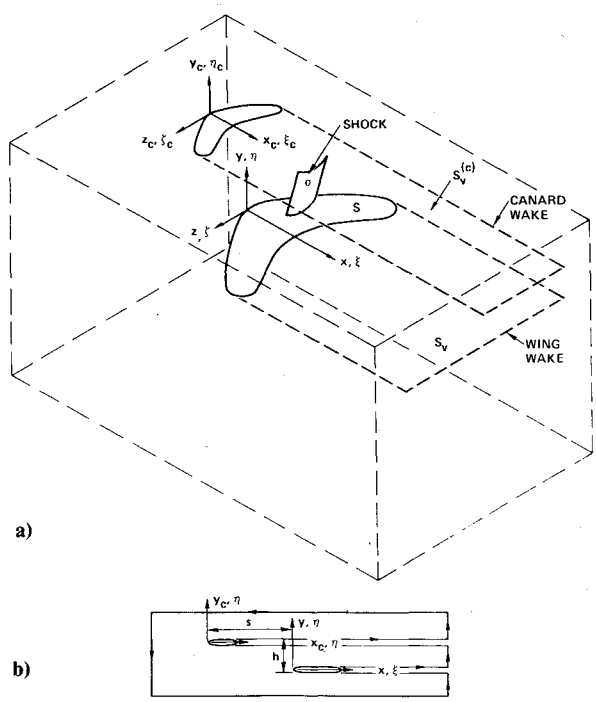

Fig. 4 a) Canard-wing system and far-field boundaries. b) Canard-wing system—profile view.

$y_c=0$ and $y=0$, yields

$$-\int\int_{S_c+S+S_v^{(c)}+S_v}[\phi]G_\zeta\,d\xi d\eta+\int\int_{S_c+S}G[\phi_\zeta]\,d\xi d\eta$$
$$=\phi(x,y,z)+A\int\int_{-\infty}^{\infty}\int\phi_\xi^2G_\xi\,d\xi d\eta d\zeta \tag{8}$$

where, in the partial integrations, all terms from the shock surfaces such as σ (shown schematically in Fig. 4a) vanish, and

$$[f(x,y,z)]\equiv f(x,y,0+)-f(x,y,0-)$$

and the ξ, ζ subscripts denote partial differentiation in the integrals.

The integrals over the finite domains can be simplified by approximating the kernels for $x^2+y^2+z^2\to\infty$ with normalized semispan $B=\mathcal{O}(y^2+z^2)$. This approximation and the condition that can be arbitrarily prescribed leads to the desired asymptotic formula

$$\phi=I_L+I_T+I_L^{(c)}+I_T^{(c)}+I_V \tag{9}$$

where, if the wing and canard are given by the equations

$$z=f_{u,l}(x,y) \qquad x_{LE}\le x\le x_{TE}, \qquad -B\le y\le B$$
$$z=f_{u,l}^{(c)}(x,y) \qquad x_{LE}^{(c)}\le x\le x_{TE}^{(c)}, \qquad -B_c\le y\le B_c$$

respectively, then

$$I_L=(z\Gamma/4\pi\rho^2)\,[1+x/R_0] \tag{10a}$$

is the wing lift contribution;

$$I_T=(x/2\pi R_0^3)\int_S\int t(\xi,\eta)\,d\xi d\eta \tag{10b}$$

is the thickness contribution;

$$I_V=-A\int\int_{-\infty}^{\infty}\int\Phi_\xi^2G_\xi\,d\xi d\eta d\zeta \tag{10c}$$

is the nonlinear source;

$$I_L^{(c)}=(z_c\Gamma_c/4\pi\rho)\,[1+x_c/R_c] \tag{10d}$$

is the canard lift; and

$$I_T^{(c)}=(x_c/2\pi R_{c_0}^3)\int_{S_c}\int t_c\,d\xi d\eta \tag{10e}$$

is the canard thickness, with

$$x_c=x-s \qquad z_c=z-h \qquad \rho^2=x^2+z^2 \qquad \rho_c^2=x_c^2+z_c^2$$
$$t=f_u-f_l \qquad t_c=f_u^{(c)}-f_l^{(c)} \qquad R^2=(x-\xi)^2+(y-\eta)^2+z^2$$
$$R_0^2=x^2+y^2+z^2 \qquad R_{c_0}^2=x_c^2+y^2+z_c^2 \qquad \Gamma=\int_{-B}^{B}\gamma(\eta)\,d\eta$$
$$\Gamma_c=\int_{-B}^{B_c}\gamma_c(\eta)\,d\eta \qquad \gamma=[\phi]_{x_{TE}} \qquad \gamma_c=[\phi]_{x_{c_{TE}}}$$

and B and B_c representing respectively the scaled wing and canard semispans.

Note that in Eq. (9)

$$I_L=\mathcal{O}(S/R_0)$$
$$I_L^{(c)}=\mathcal{O}(S_c/R_0)$$

as $R_0\to\infty$; and the rest of the terms are higher-order, being $\mathcal{O}(R_0^{-2})$, which can be neglected for sufficiently large computational domains. It is therefore apparent that owing to the linearity of the far field, the dominant effect is the sum of the two lift contributions I_L and $I_L^{(c)}$. In the two-dimensional

case discussed in Ref. 2, there is, however, nonlinear coupling between the circulations Γ and Γ_c.

In a similar fashion, the effect of the far field of a slender body contribution can be added to Eq. (9) using the nonlinear line source far-field expression given in Ref. 7. Denoting this term as I_F, we have that

$$I_F = \mathcal{O}(S_0/R_0) \quad \text{as} \quad R_0 \to \infty$$

where S_0 is the body base area. If, as in typical cases, $S_0/S_c \ll 1$ and $S_c \ll S$, then I_F will be neglected.

In the vicinity of the projections of the lifting elements in the Trefftz plane, the previous approximations become invalid. The appropriate limits are obtained by assuming

$$z, y, z_c = \mathcal{O}(B, B_c) \quad \text{as} \quad x \to \infty \tag{11}$$

Using the limit equation (11), Eq. (8) can be approximated to give the contribution of the projection of the vortex sheets from both elements,

$$\phi \doteq \frac{z_c}{2\pi} \int_{-B_c}^{B_c} \frac{\gamma_c(\eta)\,d\eta}{(y-\eta)^2 + z_c^2} + \frac{z}{2\pi} \int_{-B_w}^{B_w} \frac{\gamma(\eta)\,d\eta}{(y-\eta)^2 + z^2} \quad \text{as} \quad x \to \infty \tag{12}$$

Since

$$\lim_{z \to 0} \left\{ \frac{z}{\pi[(y-\eta)^2 + z^2]} \right\} = \delta(y-\eta)\,\mathrm{sgn} z$$

then

$$\phi(x, y, 0\pm) \doteq \frac{z_c}{2\pi} \int_{-B_c}^{B_c} \frac{\gamma_c(\eta)\,d\eta}{(y-\eta)^2 + z_c^2} \pm \frac{\gamma(y)}{2} \quad x \to \infty \tag{13a}$$

and

$$\phi(x, y, h\pm) \doteq \pm \frac{\gamma_c(y)}{2} + \frac{z}{2\pi} \int_{-B}^{B} \frac{\gamma(\eta)\,d\eta}{(y-\eta)^2 + z^2} \quad x \to \infty \tag{13b}$$

for the fuselage absent.

Equation (12) corresponds to the solution of the cross-flow Laplace's equation for the perturbation potential in the Trefftz plane cut about the projections of the wing and canard. If a fuselage is present, the solution can be obtained by superposing the appropriate Trefftz plane limit of the nonlinear line source described in Ref. 7.

Results

All the canard-wing calculations presented here were performed using the LBL CDC 7600 machine. A single fine grid encompassing both the canard and wing was used, since the configurations considered in this paper were all very closely coupled canard systems. A typical fine grid consisted of $90 \times 30 \times 20$ points and the crude grid $30 \times 20 \times 20$ points. A total of 100 crude/fine cycles requiring 10-15 min of CPU time usually resulted in satisfactory convergence in which the difference in ϕ between two successive cycles was of the order of 10^{-4}.

Gloss and Washburn[1] have made extensive experimental measurements on the close coupled canard-wing configuration shown in Fig. 5. The wing and canard surfaces consisted of sharp leading-edge circular arc airfoils. The pressure data in their report clearly indicate a strong leading-edge vortex system especially at higher angles of attack. Since the computational model in its present form cannot predict leading-edge vortex flows, for comparison purposes, only the small angle of attack case is considered, where the leading-edge vortex is weak. Figure 6 shows the comparison of spanload distribution on the wing with and without the presence of the canard. To match the experimental lift, the computer code was run at an angle of attack of 5.8 deg, while the experiment was conducted at 4.12 deg. The increased angle of attack used in the computational run is an empirical fix to account for the suction peak associated with the weak leading-edge vortex present in the experimental run, as well as viscous and wall interference effects. Even so, there is a discrepancy in the surface pressure distribution comparison between numerical prediction and experimental data, as shown in Fig. 7. The presence of the canard produces a downwash field in front of the wing, causing an effective decrease in the angle of attack. This results in a reduction in the nose pressure distribution. The comparison on the lower surface pressure with and without the canard is very good. At

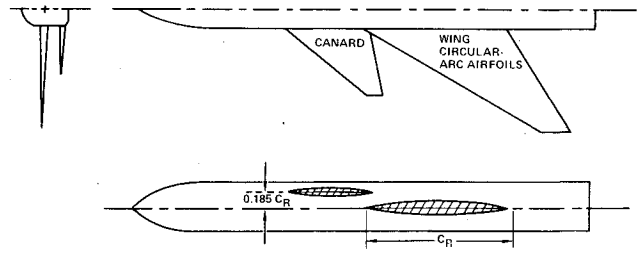

Fig. 5 Closely coupled canard-wing model (Ref. 1).

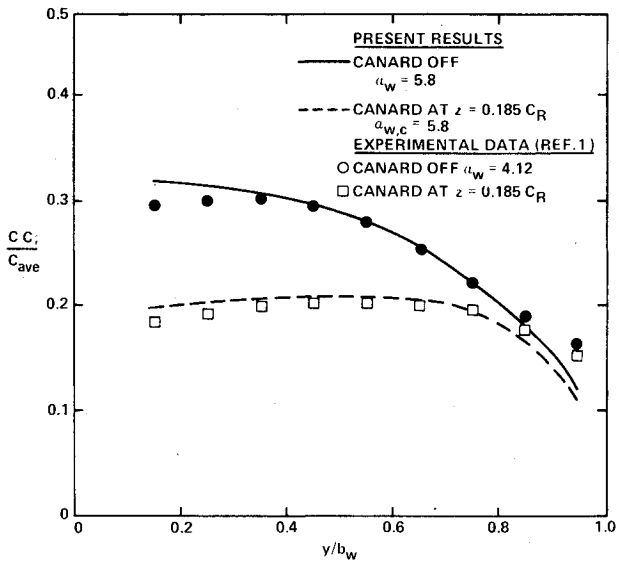

Fig. 6 Effect of canard on spanload distribution; $M_\infty = 0.95$.

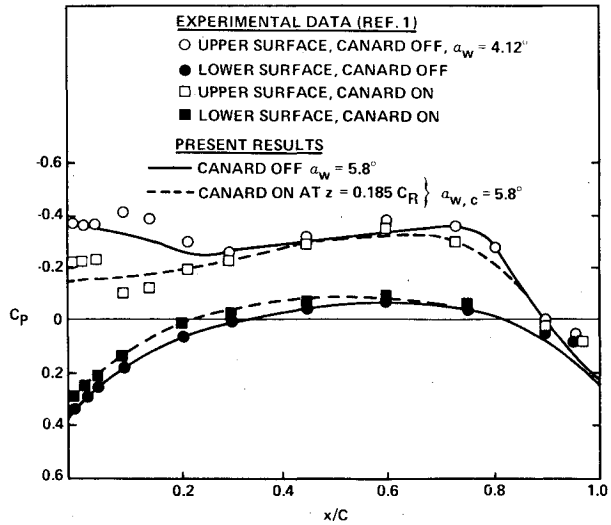

Fig. 7 Effect of canard on wing surface pressures; $y/b_w = 0.45$, $M_\infty = 0.95$.

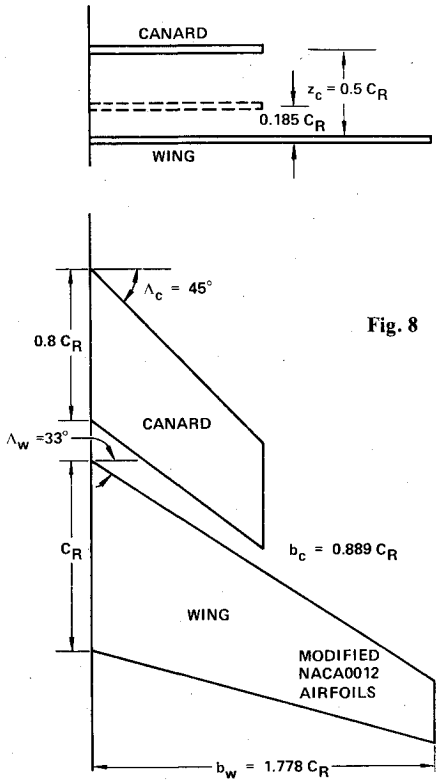

Fig. 8 Canard-wing geometry.

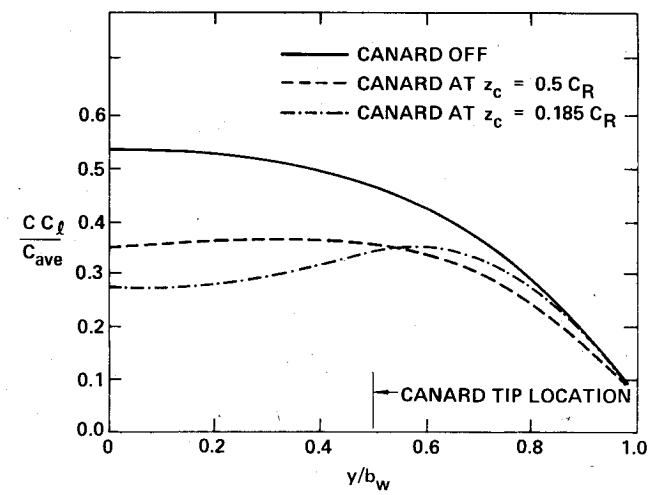

Fig. 9 Wing sectional characteristics with canard off and on; $M_\infty = 0.84$, $\alpha_{c,w} = 3$ deg.

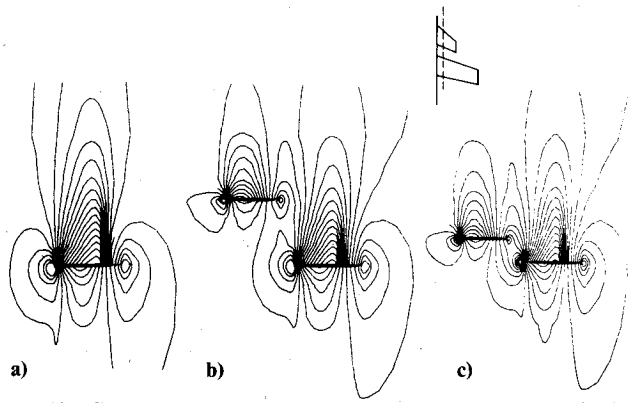

Fig. 10 Constant pressure contours at span station $y/b_w = 0.245$; $M_\infty = 0.84$, $\alpha_{w,c} = 3$ deg. a) Wing alone. b) Canard at $z_c = 0.5\ C_R$. c) Canard at $z_c = 0.185\ C_R$.

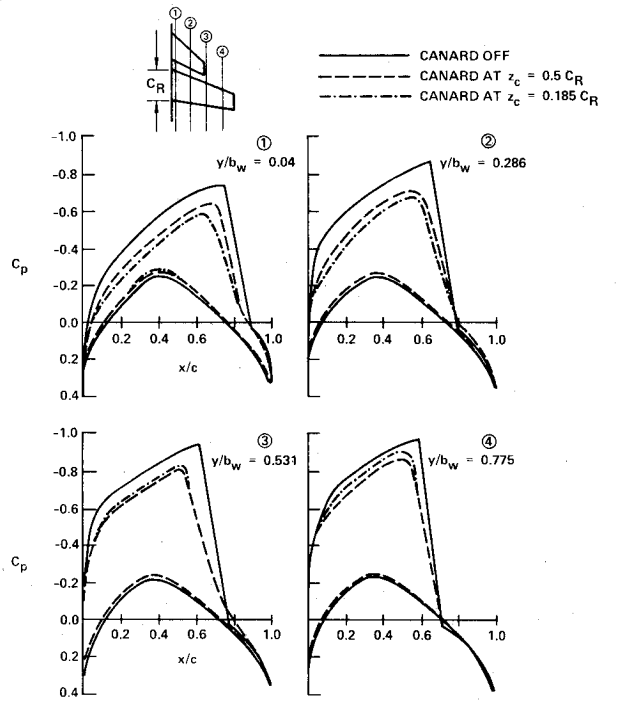

Fig. 11 Surface pressure distribution on the wing with canard off and on; $M_\infty = 0.84$, $\alpha_{c,w} = 3$ deg.

higher angles of attack the comparison with data is very poor owing to the inability of the computational model to predict the leading vortex system. The case shown in Fig. 7 at least indicates the right trend predicted by the computational model with the canard present and, interestingly, is in qualitative agreement with the behavior of two-dimensional systems treated in Ref. 2.

Another canard-wing configuration considered is shown in Fig. 8. Two different canard positions in the vertical direction are analyzed. For this case, the effect of the canard and its position on the wing sectional lift characteristics is shown in Fig. 9, for $M_\infty = 0.84$ and angle of attack of 3 deg. The lift produced by the canard produces a downwash in front of the wing causing the wing lift to decrease; however, at wing span stations away from the canard tip, the effect of the canard is minimal. Corresponding to this case, the pressure contours at the wing span station $y/b_w = 0.245$ are shown in Fig. 10 for both the canard-off and -on situations. Figure 10a shows the isolated wing case (canard off) exhibiting a shock on the upper surface. When the canard is placed at $0.5\ C_R$ above the wing plane (C_R is the wing root chord), the shock weakening on the wing due to downwash produced by the canard is clear in Fig. 10b. Even further weakening of the shock due to closer positioning of the canard is seen in Fig. 10c. Figure 11 shows the surface stations with canard off and on. This figure also clearly shows the reduction in wing shock strength when the canard is present.

Conclusions

A simple canard-wing transonic computational model is presented. The formulation neglects wake deflection, vortex roll-up, and leading-edge separation phenomena. An appropriate far-field expression for the velocity potential is derived and implemented. Results are presented for two canard-wing configurations and some comparison with experimental data is made. An empirical incidence correction for the wing leading-edge vortex gives good agreement with experiment at low incidences. The presence of the canard produces a downwash field that tends to weaken the shock system on the wing surface.

Acknowledgment

A portion of the research described in this paper was supported under AFOSR Contract F44620-81-C-0044.

References

[1] Gloss, B.B. and Washburn, K.E., "A Study of Canard-Wing Interference Using Experimental Pressure Data at Transonic Speeds," NASA TP-1355, Jan. 1979.

[2] Shankar, V. and Malmuth, N.D., "Transonic Flow Calculations over Two-Dimensional Canard-Wing Systems," *Journal of Aircraft,* Vol. 18, Feb. 1981, pp. 108-114.

[3] Shankar, V., Malmuth, N.D., and Cole, J.D., "Computational Transonic Design Procedure for Three-Dimensional Wings and Wing-Body Combinations," Paper 79-0344 presented at the AIAA 17th Aerospace Sciences Meeting, New Orleans, La., Jan. 15-17, 1979.

[4] Boppe, C.W. and Stern, M.A., "Simulated Transonic Flows for Aircraft with Nacelles, Pylons and Winglets," Paper 80-0130 presented at the AIAA 18th Aerospace Sciences Meeting, Pasadena, Calif., Jan. 14-16, 1980.

[5] Murman, E.M. and Cole, J.D., "Calculations of Plane Steady Transonic Flows," *AIAA Journal,* Vol. 9, Jan. 1971, pp. 114-121.

[6] Klunker, E.R., "Contributions to Methods for Calculating the Flow About Thin Lifting Wings at Transonic Speeds—Analytical Expression for the Far Field," NASA TN D-6530, 1971.

[7] Krupp, J.A. and Murman, E.M., "Computation of Transonic Flows over Lifting Airfoils and Slender Bodies," *AIAA Journal,* Vol. 10, July 1971, pp. 880-885.